

SCIENTIFIC REPORTS



OPEN

Atomic insight to lattice distortions caused by carrier self-trapping in oxide materials

Felix Freytag¹, Gábor Corradi² & Mirco Imlau¹

Received: 09 June 2016

Accepted: 21 October 2016

Published: 14 November 2016

We gain hitherto missing access to the spatio-temporal evolution of lattice distortions caused by carrier self-trapping in the class of oxide materials - and beyond. The joint experimental/theoretical tool introduced combines femtosecond mid-infrared probe spectroscopy with potential landscape modeling and is based on the original approach that the vibration mode of a biatomic molecule is capable to probe strongly localized, short-lived lattice distortions in its neighborhood. Optically generated, small, strong-coupling polarons in lithium niobate, mediated by OH⁻ ions present as ubiquitous impurities, serve as a prominent example. Polaron trapping is found to result in an experimentally determined redshift of the OH⁻ stretching mode amounting to $\Delta\nu_{\text{vib}} = -3 \text{ cm}^{-1}$, that is successfully modeled by a static Morse potential modified by Coulomb potential changes due to the displacements of the surrounding ions and the trapped charge carrier. The evolution of the trapping process can also be highlighted by monitoring the dynamics of the vibrational shift making the method an important tool for studying various systems and applications.

Self-trapping by electron- or hole-phonon-coupling, commonly described as small polaron formation¹, is increasingly considered in the modeling of transport phenomena in oxide materials such as superconductivity in cuprates², semiconduction in transition metal oxides³, colossal magnetoresistance in manganites^{4,5}, and also for the mechanism of photocatalysis in TiO₂⁶. In this connection, a detailed knowledge on the lattice distortions related to self-trapping, and in particular on the respective dynamics at elevated temperatures, are of major importance; however, no adequate experimental tools have been described in the literature, so far. Only recently, first attempts for a direct view on small polarons on the surface of TiO₂ have been reported by Setvin *et al.* based on a combination of scanning tunneling microscopy/spectroscopy and density functional theory⁷. In turn, Sezen *et al.* applied infrared reflection-absorption spectroscopy at low temperatures to study photoexcited polarons in zinc oxide (ZnO)⁸. By contrast, in this article, we intend to access optically generated, small polarons in the crystal bulk at room temperature and propose a time-resolved vibrational method to experimentally achieve local information on small polarons at this temperature.

Our study is performed with nominally undoped, near stoichiometric lithium niobate (LiNbO₃, LN) as a prototypical oxide material that allows for the optical generation of various kinds of short-lived small, strong-coupling electron and hole polarons⁹, i.e., self-trapped carriers with associated distortions strongly confined to a single lattice site¹. A multitude of knowledge based on a variety of experimental techniques has been gathered to access small polarons in LN in the past decades. Structural (steady-state) parameters are obtained using a combination of X-ray diffraction/Electron Paramagnetic Resonance (EPR)/Electron Nuclear Double Resonance (ENDOR)/Angle-resolved Photoemission Spectroscopy (APRES) measurements¹⁰⁻¹⁴, which, however, are limited to low temperatures and systems having appropriate spin. Information on the electronic structure is best modeled by *ab initio* techniques¹⁵, or, from the experimental viewpoint, using optical pump-probe techniques in the visible spectral range⁹. Access to the dynamics of lattice distortions due to the self-trapping of optically excited carriers, is of importance in LN to foster the understanding of the bulk photovoltaic effect and its small polaron based microscopic modeling¹⁶.

Our original approach makes use of a molecular ligand in direct vicinity of the small polaron site such that its vibrational spectroscopic fingerprint $E_{\text{vib}} = h\nu_{\text{vib}}$ changes by $\Delta\nu_{\text{vib}}$ due to a modified electrostatic potential in

¹Osnabrueck University, School of Physics, Barbarastrasse 7, 49076 Osnabrueck, Germany. ²Wigner Research Centre for Physics, Institute for Solid State Physics and Optics, Hungarian Academy of Sciences, Konkoly-Thege u. 29-33, 1121 Budapest, Hungary. Correspondence and requests for materials should be addressed to F.F. (email: felix.freytag@uni-osnabrueck.de)

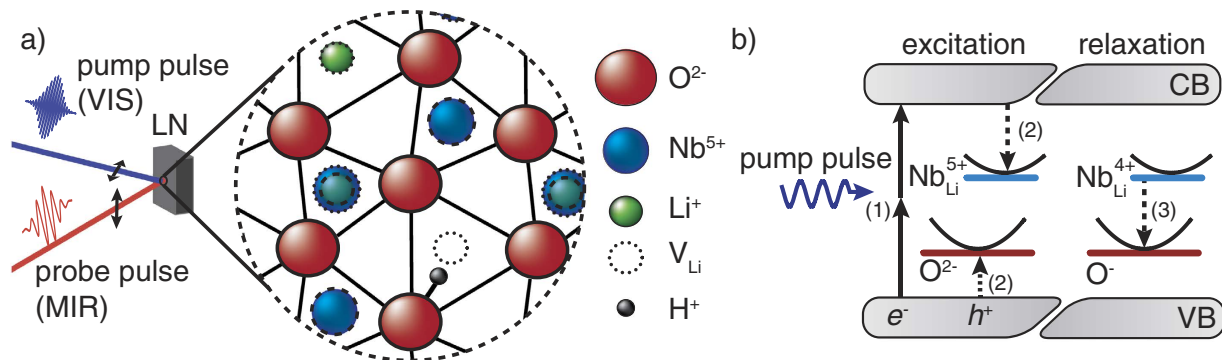


Figure 1. (a) Structure of the oxygen plane of LiNbO₃¹⁰ (dotted: cations above plane, dashed: below plane) and schematic setup. (b) Electronic transition: (1) two-photon-absorption, (2) generation of small Nb_{Li}⁴⁺ electron and O⁻ hole polarons ($\tau < 1$ ps)⁴¹, (3) recombination ($\tau \approx 1$ s) (Table 1).

the presence of a short-range lattice displacement. With knowledge on the lattice position of both the molecular ligand and the small polaron site, the structural distortion can be reconstructed from the measurement of $\Delta\nu_{\text{vib}}$. Thus, a variety of small polaron features like the associated displacements of atomic equilibrium positions or the electron-phonon coupling strength can be obtained. A particular strength of the approach is the possibility to study the temporal evolution of localized atomic displacements if dynamic measurements for the detection of $\Delta\nu_{\text{vib}}(t)$ are applied. Here we use a femtosecond visible pump, mid-infrared (MIR) probe absorption spectrometer (cf. e.g. ref. 17) with a remarkable shot-to-shot sensitivity below 10^{-3} OD (Optical Density) at a spectral and temporal resolution of $\delta\nu_{\text{vib}}(t)/\nu_{\text{vib}} \approx 9 \cdot 10^{-4}$, and $\delta t = 1$ ms, respectively. It is shown that the transient absorption spectrum $\Delta A(\nu, t) = A(\nu, t)_{\text{pumped}} - A(\nu, t)$ reveals a frequency shift of $\Delta\nu_{\text{vib}}(\text{OH}^-)$ upon light exposure that can be related to the formation of short-lived, small O⁻ hole polarons. Furthermore, the dynamic features from ms to seconds in the dark resemble the well-known stretched-exponential behavior that is characteristic for hopping-transport¹⁸. The main purpose of this article is (i) to verify the underlying experimental approach, i.e., to demonstrate and explain the small polaron access using changes in a vibrational fingerprint, (ii) to sketch the physical relation between experimentally determined frequency shifts and the structural properties of small, strong-coupling polarons, and (iii) to show-up the possibility for dynamic measurements with small polaron hopping-transport as an example.

Fundamentals

Carrier self trapping in lithium niobate. In what follows, we will focus on small, strong-coupling O⁻ hole polarons (HP)¹⁹ in direct vicinity to a V_{Li} vacancy as well as on Nb_{Li}⁴⁺ electron polarons (GP)²⁰. Structural details of the oxygen plane of LN are depicted in Fig. 1a. In both cases the trapped charge can be transferred by light to a neighboring equivalent or nearly equivalent site, thereby stripping the trapped charge of its polarization halo^{18,19}. This results in broad absorption features playing a central role in the study and application of dynamic properties of small polarons in LN⁹. The absorption maxima are reported in the visible region (VIS, 2.5 eV; $\approx 20,000$ cm⁻¹) for HP and in the near infrared (NIR, 1.6 eV; $\approx 13,000$ cm⁻¹) for GP. In nominally undoped LN, pairs of HP and GP can be generated via two-photon excitation at 2.5 eV (cf. Fig. 1b, left part), i.e., with photon energies much below the band edge energy ($E_{\text{gap}} \approx 4.1$ eV²¹). To raise signal changes in the MIR range (≈ 10 mOD, see below), it is necessary to generate a large number density $N_{\text{sp}} > 10^{18}$ cm⁻³ of small polarons. This is realized by using intense laser pulses ($I_{\text{pump}} = (500 \pm 100)$ TW/m², extraordinary light polarization) with sub-ps pulse duration ($\tau_{\text{pump}} = (120 \pm 10)$ fs), as N_{sp} depends quadratically on the intensity of the pump-pulse, $N_{\text{sp}} = \text{const} \cdot I_{\text{pump}}^2$ ²², but also on the pulse duration τ_{pump} ²³. Furthermore, repetitive fs-pulse exposure ($f_{\text{rep}} = 1$ kHz) is applied, which leads, after a few seconds of illumination, to a saturation of the MIR effect. The average small polaron lifetimes $\tau_{\text{GP}} \approx \tau_{\text{HP}} \approx (1.1 \pm 0.3)$ s $\gg 1/f_{\text{rep}}$ accord with the mutual HP-GP-recombination path, as shown in Fig. 1b, right part.

Hydroxide ions as a molecular probe. Hydroxide ions, OH⁻¹³, inevitably introduced during crystal growth are used as molecular probes. Real position and vibrational properties have been studied in LN crystals comprehensively (for reviews, cf. refs 24 and 25), showing that H⁺ is bound to one of the O²⁻ neighbors of a V_{Li}²⁶⁻²⁸ (note that $c_{\text{V}_{\text{Li}}} \gg c_{\text{H}^+}$ ²⁶). Due to the dipolar character of this defect complex it may be assumed that light-induced, small polarons are formed or get temporarily trapped in its direct vicinity. We consider an O⁻ hole polaron localized at an oxygen ion next to the same V_{Li} (see Fig. 1a). It is already established that the energy of the OH⁻-stretching vibration depends on the surroundings of the particular OH⁻-site resulting in several components of its MIR absorption feature. In as-grown, near stoichiometric LN up to five distinct bands have been observed^{29,30}, the most prominent bands appear at 3,466 cm⁻¹, 3,480 cm⁻¹, and 3,490 cm⁻¹ (see Fig. 2a) with the lowest vibrational energy related to the O²⁻ sites closest to V_{Li}²⁶. To observe pump-induced frequency changes of the OH⁻-stretching bond, we use probe pulses with a spectral width of $\Delta\tilde{\nu} \approx 200$ cm⁻¹ at a center wavenumber of $\tilde{\nu} = 3,484$ cm⁻¹ ($I = 0.03$ TW/m², $\tau_{\text{probe}} = (230 \pm 20)$ fs, $f_{\text{rep}} = 1$ kHz, ordinary light polarization). All studies

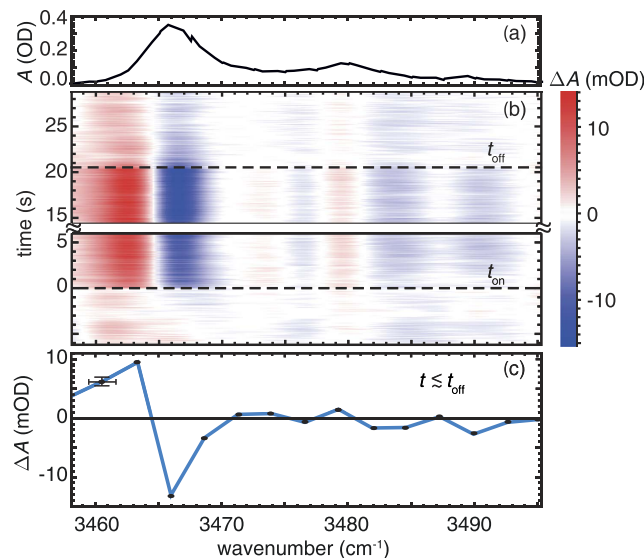


Figure 2. (a) Steady state spectrum of the OH⁻-stretching absorption feature in nearly stoichiometric lithium niobate. (b) Time dependent change of the absorption $\Delta A(\bar{\nu}, t)$ of the OH⁻-stretching vibration. t_{on} and t_{off} denote the times where repetitive pump-pulse exposure is switched on and off. (c) Spectrum of the absorption change at $t = t_{\text{off}}$ (black data points). The blue line is a guide to the eye; its shape indicates a frequency shift of the prominent absorption feature by -3 cm^{-1} .

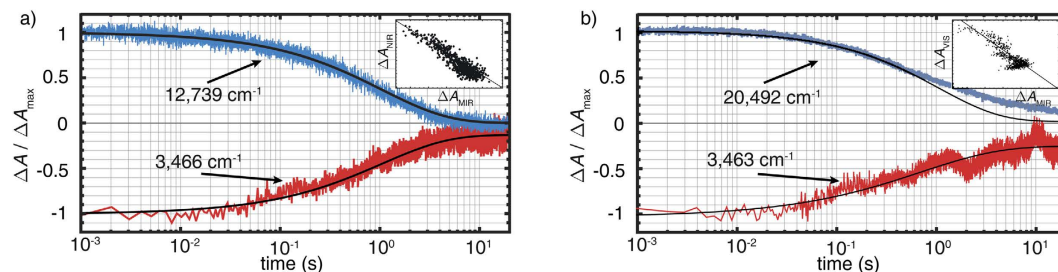


Figure 3. Relaxation dynamics probed at (a) $3,466 \text{ cm}^{-1}$ (MIR) and $12,739 \text{ cm}^{-1}$ ($\lambda = 785 \text{ nm}$, NIR) and (b) at $3,463 \text{ cm}^{-1}$ (MIR, inverted) and $20,492 \text{ cm}^{-1}$ ($\lambda = 488 \text{ nm}$, VIS). The solid lines indicate the results of fitting stretched exponential functions to the data sets. Insert: Plot of the absorbance change (a) ΔA_{NIR} , (b) ΔA_{VIS} as a function of ΔA_{MIR} ; a linear dependence is revealed over the entire data range.

were performed with an X-cut sample (aperture $10 \times 9 \text{ mm}^2$, thickness 2 mm) with a [Li]/[Nb] ratio of 0.992³¹ and a hydrogen concentration³² of $\approx 3 \cdot 10^{18} \text{ cm}^{-3}$.

Results

Experiment. The time dependent change of the absorption feature $\Delta A(\bar{\nu}, t)$ in the region of $\nu_{\text{vib}}(\text{OH}^-)$ is plotted as a function of wavenumber $\bar{\nu}$ in Fig. 2b using the color coding: red for $\Delta A(\bar{\nu}, t) > 0$ and blue for $\Delta A(\bar{\nu}, t) < 0$. In the time regime $t < t_{\text{on}}$, i.e., without the presence of the pump-pulse, we detect a weak background signal that is applied for signal correction. At t_{on} , the repetitive pump-pulse exposure is switched on and induces spectral changes $\Delta A(\bar{\nu}, t)$ well above the noise limit. The temporal evolution resembles a mono-exponential behavior with a characteristic time constant in the order of 100 ms. The spectral evolution shows changes in the shape of all three MIR absorption bands with maximum values of about -14 mOD at $3,466 \text{ cm}^{-1}$ and about $+10 \text{ mOD}$ at $3,463 \text{ cm}^{-1}$. Pump-induced changes at $3,480 \text{ cm}^{-1}$ and $3,490 \text{ cm}^{-1}$ are also observed but do not exceed 2 mOD; accordingly we will focus in the following on the strongest absorption band. Switching off the pump-pulse exposure ($t > t_{\text{off}}$), the absorption change decays to nearly zero and the process can be repeated from the beginning. Exemplarily, the spectrum $\Delta A(\bar{\nu}, t = t_{\text{off}})$ is extracted and plotted in Fig. 2c. The remarkable shape, in particular in the region of the strongest absorption band, can be understood as a shift of the OH⁻ absorption frequency by -3 cm^{-1} to $3,463 \text{ cm}^{-1}$.

The next step is to verify the relation of this shift to the presence of small, strong-coupling polarons. For this purpose, the temporal relaxation dynamics in the mid-infrared spectral range is highlighted in a semi-logarithmic plot in Fig. 3 (red data points) and compared with the temporal decay dynamics of the light-induced absorption detected in the near-infrared and visible spectral range (blue data points) close to the maximum of the GP and

Probed effect	Range	$\nu_{\text{probe}}/\text{cm}^{-1}$	τ/s	β
Molecular vibration	MIR	3,463	0.7 (4)	0.55 (10)
		3,466	1.0 (4)	0.65 (10)
Electronic transition	NIR	12,739	1.1 (3)	0.65 (10)
	VIS	20,492	1.1 (3)	0.70 (10)

Table 1. Results of fitting a stretched-exponential function to the temporal dynamics in the VIS, NIR and MIR spectral range (cf. straight lines in Fig. 3).

HP absorption features. It is evident from Fig. 3 that the temporal behaviors of the absorption changes in all spectral ranges are strongly correlated, despite the differences in the sign of ΔA . As shown in the inserts of Fig. 3, the $\Delta A_{\text{NIR/VIS}}(\Delta A_{\text{MIR}})$ plot is essentially linear. For a quantitative comparison, a stretched-exponential function

$$\Delta A(t) = A(0) \cdot \exp[-(t/\tau)^\beta] + \text{const.} \quad (1)$$

with time constant τ and stretching exponent β is fitted to each data set. The values (τ, β) obtained from fitting the experimental data are listed in Table 1 and are comparable within the error margins. These findings are particularly remarkable since the absorption in the NIR and VIS region is related to changes in the electronic structure, whereas the absorption in the MIR is characteristic for the molecular vibration of OH^- . The linear relation between the signals of different origin, thus, gives clear evidence for their common physical background which is the hopping transport of GP and HP leading to their recombination (cf. Fig. 1b). We note that the absorption dynamics at $3,463 \text{ cm}^{-1}$ in Fig. 3b shows a reduced signal-to-noise ratio in comparison with data at $3,466 \text{ cm}^{-1}$, that is due to the lower signal level at this wavenumber. Concerning the dynamics at $20,492 \text{ cm}^{-1}$, a slight variation to long decay times in comparison to the stretched-exponential decay is observed, that may be attributed to the presence of $\text{Fe}_{\text{Li}}^{3+}$ impurities, always present in the ppm regime in nominally undoped lithium niobate and acting as deep electron traps. At the same time, the frequency shift cannot be explained by other defect centers such as extrinsic dopants, as a change in the cation environment, caused, e.g., by doping, leads to a blue shift of the MIR absorption spectrum (e.g. magnesium, indium or neodymium shift the frequency by a few $+10 \text{ cm}^{-1}$ ^{25,33}). Electron polarons bound to $\text{Nb}_{\text{Li}}^{5+}$ antisites can be discarded in this respect as protons are not expected to associate with antisites due to the huge surplus positive charge of the latter. Small, free polarons on a nearby regular $\text{Nb}_{\text{Nb}}^{5+}$ -site would have much shorter relaxation times ($\tau \approx 1 \mu\text{s}$)³⁴ and can also be excluded.

Theory. In the final part of this letter, based on the experimental findings, we give an estimate of the local lattice distortion induced by small hole polarons, using a simple point charge approximation for the change of the crystal field and a static Morse potential³⁵ along the OH^- -bond with the anharmonicity constant $\omega_e x_e$:

$$\begin{aligned} V(r)^{\text{Morse}} &= D_e \cdot (e^{-2a(r-r_0)} - 2e^{-a(r-r_0)}) \\ \omega_e &= \frac{a}{2\pi c} \sqrt{\frac{2D_e}{\mu}}, \\ x_e &= hc \frac{\omega_e}{4D_e} \end{aligned}$$

with D_e being the dissociation energy, a the stretching constant, r_0 the O-H distance with the lowest potential energy and $\mu = \frac{m_p m_o}{m_o + m_p}$ the reduced proton mass. In the absence of polarons the values of D_e and a can be found using measured frequencies ($\nu_{0,1} = \omega_e - 2\omega_e x_e = 3,466 \text{ cm}^{-1}$, $\nu_{0,2} = 6,745 \text{ cm}^{-1}$) of the OH^- -stretching vibration³⁶. A hole polaron is added at another oxygen neighbor of the lithium vacancy out of the three nearest ones. The potential change seen by the proton is accounted for by the Coulomb potential due to the added point charge on its host ion *and* by the changes of the Coulomb potentials due to the displacements of all neighboring ions with the exception of the oxygen in OH^- . For simplicity the displacements are assumed to be radial (with respect to the polaron host) and scaled by the factor q_i/d_i where q_i is the charge and d_i the distance (to the host) of the i^{th} neighbor (see Fig. 4). This scaling corresponds to considering only long range electron-phonon interaction characterized by the static dielectric constant ε_0 having a large value in comparison to the optical dielectric constant ε_∞ ($\varepsilon_{0,11}/\varepsilon_\infty = 57.6$, $\varepsilon_{0,33}/\varepsilon_\infty = 19.0$ ³⁷, with $\varepsilon_\infty \approx 1.47 \cdot \varepsilon_{\text{vacuum}}$ ³⁸) in LN. Choosing the displacement δd_{Nb} of the nearest Nb neighbor ($d_{\text{Nb}^{5+}-\text{O}^{2-}} = 0.188 \text{ nm}$) as a numerical scaling parameter and neglecting possible changes of the OH^- -direction, the resulting potential along the bond can be approximated by a new Morse potential of the same type.

The three dimensional Coulomb potential is calculated for a $5 \times 5 \times 2$ hexagonal unit cell (1588 atoms), using the structural data of the LiNbO_3 lattice¹⁰ with a lithium and an adjacent oxygen ion at the center of the cell replaced by an OH^- -molecular-ion represented by a static Morse potential. The site of the proton substituting V_{Li} is assumed to be in the bisecting plane of the largest oxygen triangle (O-O distance 336 pm)²⁸ with an O-H bond length of 98.8 pm and an out-of-plane angle of 4.3 degrees towards V_{Li} ²⁷. We note that a $\text{OH}^- - \text{V}_{\text{Li}}$ -complex causes only negligible distortions of the lattice as calculated by Lengyel *et al.*^{25,27}. Cation charges in the boundary area of the cell are reduced to secure an overall neutral charge. The changes of the potential along the direction of the O-H bond resulting from the presence of a hole polaron are added to the Morse potential, neglecting the difference between the center of mass of OH^- and the corresponding oxygen site. The hole polaron state is modeled

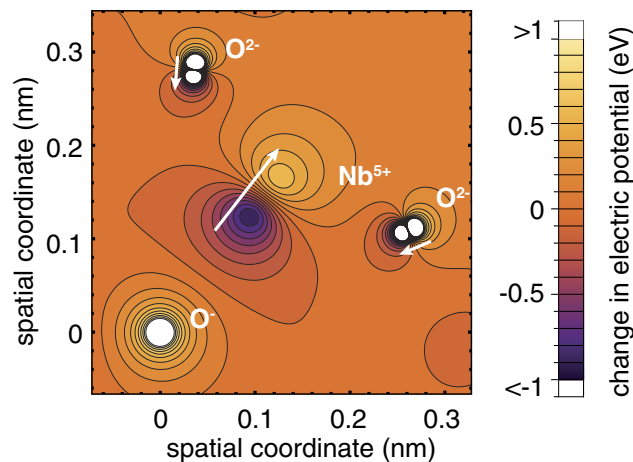


Figure 4. Electrostatic potential change in the oxygen plane of LiNbO_3 calculated for a polaronic distortion corresponding to a redshift of -3 cm^{-1} of the OH^- -stretching vibration. Arrows (enlarged) indicate amplitudes and directions of displacements (projected to the oxygen plane) of close Nb^{5+} and O^- neighbors of the polaron host that is positioned in the origin. Note that the Nb^{5+} site is $\approx 0.088 \text{ nm}$ below the oxygen plane.

by an additional positive charge localized at one of the oxygen atoms in closest vicinity to the V_{Li} -site and by scaled displacements of the surrounding atoms within a radius of 5 \AA .

For $\delta d_{\text{Nb}} = 0.024 \text{ nm}$ the modified Morse potential returns the shifted fundamental frequency $3,463 \text{ cm}^{-1}$ found by our experiments. Taking into account only the point charge of the polaron without lattice relaxation, a blue shift of $+5 \text{ cm}^{-1}$ is obtained which stresses the importance of the polaronic relaxation. The obtained $\approx 12.5\%$ increase of the smallest O-Nb distance corresponds to a $\approx 1.7\%$ increase of the closest O-Li distance ($d_{\text{Li}^+-\text{O}^{2-}} = 0.245 \text{ nm}$), and an average $\approx 2.1\%$ decrease of the various O-O distances (between 0.272 nm and 0.336 nm), taking into account the adopted q_i/d_i scaling (see Fig. 4). Considering this scaling our calculations are consistent with recent ab initio studies of the polaronic deformation at the impurity site in Fe:LiNbO_3 by Sanson *et al.*³⁹ who found a $\approx 4.7\%$ decrease of the Fe-O distance ($d_{\text{Fe}^{2+}-\text{O}^{2-}} = 0.2124 \text{ nm}$) upon hole capture by Fe^{2+} , thus, supporting our model assumptions. The estimates derived from our simplified model may already serve as useful input parameters for more complex model calculations and/or as a crosscheck of the validity of various small polaron model approaches. Appropriate calculations may be used straightforwardly for the determination of further small polaron parameters, like the electron phonon coupling strength.

Summary and Conclusions

Summarizing the results, a pump-induced -3 cm^{-1} shift of the frequency of the OH^- -stretching vibration is experimentally verified and attributed to the presence of small, strong-coupling O^- hole polarons next to the OH^- ion. Sign and magnitude of the shift can only be explained by taking into account, in addition to the polaronic charge, also the distortion of the lattice in the imminent neighborhood - a very striking result that supports the microscopic approach for the bulk photovoltaic effect based on small, strong-coupling polarons in LN ¹⁶ and will foster its advances. The measured shift can be reconstructed by modeling the change of the three-dimensional Coulomb potential caused by the polaron, leading to reasonable values of the ligand displacements. The measured frequency shift may also provide a stringent test for ab initio/DFT calculations desirable for a deeper understanding of the properties of polarons interacting with molecular defects, and vice versa. It should be stressed that the presented experimental approach for determining local lattice deformation, although introduced with small, strong-coupling polarons, can also be applied for the detection of small, weak-coupling and large polarons¹. It is furthermore neither limited to the chosen molecular hydroxide group nor to lithium niobate as a host material, and may be adopted, e.g., to further oxides like TiO_2 , ZnO or MgO , but also to probe localized atomic distortions in DNA⁴⁰. As its most important aspect, however, the approach enables dynamic studies at room temperature and, thus, general physical questions about polaron formation, hopping-transport and recombination phenomena, encompassing time scales from sub-ps to seconds, become accessible. If necessary, the time resolution can be increased to the sub-ps time regime by using up-conversion MIR-spectroscopy; this enables a larger signal-to-noise ratio accompanied with a better time resolution.

References

1. Emin, D. *Polarons* (Cambridge University Press, 2013).
2. Müller, K. A. The unique properties of superconductivity in cuprates. *J. Supercond. Novel Magn.* **27**, 2163–2179 (2014).
3. Lany, S. Semiconducting transition metal oxides. *J. Phys.: Condens. Matter* **27**, 283203 (2015).
4. Salamon, M. B. & Jaime, M. The physics of manganites: Structure and transport. *Rev. Mod. Phys.* **73**, 583–628 (2001).
5. Hartinger, C., Mayr, F., Loidl, A. & Kopp, T. Polaronic excitations in colossal magnetoresistance manganite films. *Phys. Rev. B* **73**, 024408 (2006).
6. Linsebigler, A. L., Lu, G. & Yates, J. T. Photocatalysis on TiO_2 surfaces: Principles, mechanisms, and selected results. *Chem. Rev.* **95**, 735–758 (1995).
7. Setvin, M. *et al.* Direct View at Excess Electrons in TiO_2 Rutile and Anatase. *Phys. Rev. Lett.* **113**, 086402 (2014).
8. Sezen, H. *et al.* Evidence for photogenerated intermediate hole polarons in ZnO . *Nat. Commun.* **6**, 6901 (2015).

9. Imlau, M., Badorreck, H. & Merschjann, C. Optical nonlinearities of small polarons in lithium niobate. *Appl. Phys. Rev.* **2**, 040606 (2015).
10. Abrahams, S., Reddy, J. & Bernstein, J. Ferroelectric lithium niobate. 3. Single crystal X-ray diffraction study at 24 °C. *J. Phys. Chem. Solids* **27**, 997–1012 (1966).
11. Corradi, G., Söthe, H., Spaeth, J. M. & Polgár, K. Mn²⁺ defects in LiNbO₃: an electron nuclear double resonance (ENDOR) investigation of the Mn²⁺ site and the local disorder. *J. Phys.: Condens. Matter* **2**, 6603–6618 (1990).
12. Grachev, V. & Malovichko, G. EPR, ENDOR, and optical-absorption study of Cr³⁺ centers substituting for niobium in Li-rich lithium niobate crystals. *Phys. Rev. B* **62**, 7779–7790 (2000).
13. Wöhlecke, M. & Kovács, L. OH⁻ ions in Oxide Crystals. *Crit. Rev. Solid State Mater. Sci.* **26**, 1–86 (2001).
14. Moser, S. *et al.* Tunable Polaronic Conduction in Anatase TiO₂. *Phys. Rev. Lett.* **110**, 196403 (2013).
15. Nahm, H. H. & Park, C. H. First-principles study of microscopic properties of the Nb antisite in LiNbO₃: Comparison to phenomenological polaron theory. *Phys. Rev. B* **78**, 184108 (2008).
16. Schirmer, O. F., Imlau, M. & Merschjann, C. Bulk photovoltaic effect of LiNbO₃:Fe and its small-polaron-based microscopic interpretation. *Phys. Rev. B* **83**, 165106 (2011).
17. Rini, M., Kummrow, A., Dreyer, J., Nibbering, E. T. J. & Elsaesser, T. Femtosecond mid-infrared spectroscopy of condensed phase hydrogen-bonded systems as a probe of structural dynamics. *Faraday Discuss.* **122**, 27–40 (2002).
18. Berben, D. *et al.* Lifetime of small polarons in iron-doped lithium-niobate crystals. *J. Appl. Phys.* **87**, 1034 (2000).
19. Schirmer, O. F. O⁻ bound small polarons in oxide materials. *J. Phys.: Condens. Matter* **18**, R667 – R704 (2006).
20. Schirmer, O. F., Imlau, M., Merschjann, C. & Schoke, B. Electron small polarons and bipolarons in LiNbO₃. *J. Phys.: Condens. Matter* **21**, 123201 (2009).
21. Kovács, L., Ruschhaupt, G., Polgár, K., Corradi, G. & Wöhlecke, M. Composition dependence of the ultraviolet absorption edge in lithium niobate. *Appl. Phys. Lett.* **70**, 2801 (1997).
22. Merschjann, C. *et al.* Absorption cross sections and number densities of electron and hole polarons in congruently melting LiNbO₃. *J. Phys.: Condens. Matter* **21**, 015906 (2009).
23. Badorreck, H. *et al.* Scanning nonlinear absorption in lithium niobate over the time regime of small polaron formation. *Opt. Mater. Express* **5**, 2729 (2015).
24. Cabrera, J. *et al.* Hydrogen in lithium niobate. *Adv. Phys.* **45**, 342–392 (1996).
25. Lengyel, K. *et al.* Growth, defect structure, and THz application of stoichiometric lithium niobate. *Appl. Phys. Rev.* **2**, 040601 (2015).
26. Yan, W. *et al.* The H⁺ related defects involved in domain reversal for both near-stoichiometric and heavily Mg-doped lithium niobate crystals. *Eur. Phys. J. B* **43**, 347–353 (2005).
27. Lengyel, K., Timon, V., Hernandez-Laguna, A., Szalay, V. & Kovács, L. Structure of OH⁻ defects in LiNbO₃. *IOP Conf. Ser.: Mater. Sci. Eng.* **15**, 012015 (2010).
28. Nahm, H. H. & Park, C. H. Microscopic structure of hydrogen impurity in LiNbO₃. *Appl. Phys. Lett.* **78**, 3812 (2001).
29. Kovács, L., Szalay, V. & Capelletti, R. Stoichiometry dependence of the OH⁻ absorption band in LiNbO₃ crystals. *Solid State Commun.* **52**, 1029–1031 (1984).
30. Hong-Jian, C. *et al.* OH⁻ absorption bands of LiNbO₃ with varying composition. *Chin. Phys. B* **18**, 2372–2376 (2009).
31. Dravec, G. & Kovács, L. Determination of the crystal composition from the OH⁻ vibrational spectrum in lithium niobate. *Appl. Phys. B* **88**, 305–307 (2007).
32. Klauer, S., Wöhlecke, M. & Kapphan, S. Influence of H-D isotopic substitution on the protonic conductivity of LiNbO₃. *Phys. Rev. B* **45**, 2786–2799 (1992).
33. Kovács, L. *et al.* Lattice site of trivalent impurities in Mg-doped lithium niobate crystals. *Mater. Sci. Eng. B* **9**, 505–508 (1991).
34. Merschjann, C., Berben, D., Imlau, M. & Wöhlecke, M. Evidence for Two-Path Recombination of Photoinduced Small Polarons in Reduced LiNbO₃. *Phys. Rev. Lett.* **96**, 186404 (2006).
35. Morse, P. M. Diatomic Molecules According to the Wave Mechanics. II. Vibrational Levels. *Phys. Rev.* **34**, 57–64 (1929).
36. Gröne, A. & Kapphan, S. Sharp, temperature dependent OH/OD IR-absorption bands in nearly stoichiometric (VTE) LiNbO₃. *J. Phys. Chem. Solids* **56**, 687–701 (1995).
37. Smith, R. T. Temperature dependence of the elastic, piezoelectric, and dielectric constants of lithium tantalate and lithium niobate. *J. Appl. Phys.* **42**, 2219 (1971).
38. Schlarb, U. & Betzler, K. Refractive indices of lithium niobate as a function of temperature, wavelength, and composition: A generalized fit. *Phys. Rev. B* **48**, 15613–15620 (1993).
39. Sanson, A. *et al.* Polaronic deformation at the Fe^{2+/3+} impurity site in Fe:LiNbO₃ crystals. *Phys. Rev. B* **91**, 094109 (2015).
40. Alexandre, S. S., Artacho, E., Soler, J. M. & Chacham, H. Small Polarons in Dry DNA. *Phys. Rev. Lett.* **91**, 108105 (2003).
41. Yochum, H. M. *et al.* Short-pulse excitation and spectroscopy of KNbO₃, LiNbO₃, and KTiOPO₄. *Radiat. Eff. Defect S.* **150**, 271–276 (1999).

Acknowledgements

The authors gratefully acknowledge suggestions of K. Lengyel and crystal preparation by K. Polgár and coworkers at the Wigner Research Centre for Physics, Budapest, as well as discussions with S. Sanna and S. Messerschmidt. Financial support from a bilateral DAAD-MÖB project (No. 57139940 from the German and No. 65056 from the Hungarian side), the Deutsche Forschungsgemeinschaft (DFG) via projects IM37/5-2, INST 190/137-1 FUGG and INST 190/165-1 FUGG and the Open Access Publishing Fund of Osnabrueck University is kindly acknowledged.

Author Contributions

M.I. had the original idea and directed the experiments. F.F. measured and analyzed the data and drafted the text of the paper. G.C. contributed to the analysis of the data and revised the paper. All authors read, contributed and approved the final version of the manuscript.

Additional Information

Competing financial interests: The authors declare no competing financial interests.

How to cite this article: Freytag, F. *et al.* Atomic insight to lattice distortions caused by carrier self-trapping in oxide materials. *Sci. Rep.* **6**, 36929; doi: 10.1038/srep36929 (2016).

Publisher's note: Springer Nature remains neutral with regard to jurisdictional claims in published maps and institutional affiliations.



This work is licensed under a Creative Commons Attribution 4.0 International License. The images or other third party material in this article are included in the article's Creative Commons license, unless indicated otherwise in the credit line; if the material is not included under the Creative Commons license, users will need to obtain permission from the license holder to reproduce the material. To view a copy of this license, visit <http://creativecommons.org/licenses/by/4.0/>

© The Author(s) 2016